

MODEL DEFORMATION TEMPERATURES DERIVED FROM EBSD DATA FOR OLIVINE IN TYPE 6 ORDINARY CHONDRITES AND UREILITES. A. M. Ruzicka¹ and R.C. Hugo¹, ¹Cascadia Meteorite Laboratory and Department of Geology, Portland State University, Portland, OR 97207-0751, ruzickaa@pdx.edu.

Introduction: Crystal rotation misorientations within olivine can be measured with Electron Backscatter Diffraction (EBSD) techniques and used to infer dislocation slip systems and the relative temperature of deformation in type 6 ordinary chondrites [1,2]. In general, slip systems in olivine can depend on variables besides temperature, including strain rate, pressure, and water content [3,4,5], but pressure and strain rate have counterbalancing effects on activating slip systems during a shock process, and in metamorphosed ordinary chondrites water contents are low, leaving deformation temperature as the most important variable affecting slip systems in these meteorites [1]. Relative temperature can be related to an EBSD metric for olivine we designate as R_{2-10} , where $R_{2-10} = [f_{010} + f_{001}] / [f_{100} + f_{010} + f_{001}]$, and f_i is a value proportional to the frequency of crystal rotation misorientations along sub-grain boundaries with 2-10° misorientations in the $i = \langle 100 \rangle$, $\langle 010 \rangle$ and $\langle 001 \rangle$ directions of olivine [1,2]. Here we utilize data for type 6 ordinary chondrites as well as that of ureilites to estimate model temperatures of deformation in these meteorites.

CRA diagrams: f_i and therefore R_{2-10} values can be determined using crystal rotation axis (CRA) plots, which show EBSD-derived misorientation rotation directions in an olivine crystal frame (Fig. 1). With increasing temperature, slip systems should progress in sequence from the fields colored blue, green, yellow, orange and red in Fig. 1, which reflect increasing proportion of a -type slip (slip in the $[100]$ direction) to c -type slip (slip in the $[001]$ direction) [1]. R_{2-10} is sensitive to the proportion of c - and a -type slip, the main temperature indicator, but does not specifically take into account the possibility of rotations occurring in other directions, nor the difference in temperature expected for rotations at the $\langle 010 \rangle$ and $\langle 100 \rangle$ poles (which are lumped together in the parameter). Here we use large area map (LAM) EBSD data for type 6 ordinary chondrites, and for the coarse and fine fractions of ureilites (three ‘normal’ textured, including Northwest Africa (NWA) 11993, NWA 12433, and NWA 7630; and one recrystallized, including NWA 7304). We contoured CRA data using 25° half-widths, to emphasize broad trends, and obtained large datasets (e.g., $\sim 10^5$ pixels) of 2-10° misorientation rotations, to ensure that signatures are representative.

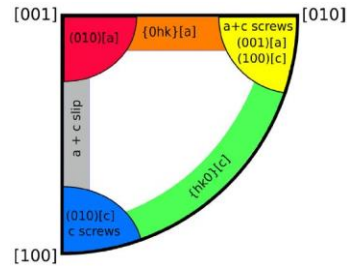


Fig. 1. Schematic CRA diagram for olivine showing slip systems; color connotes deformation temperature (e.g., blue=cold, red=hot) [after 1,2].

Approach: Our model assumes that temperature is the chief control on slip systems in olivine. We establish benchmarks for meteorites with low and high R_{2-10} and independent estimates of the temperatures at which these were deformed. The low-temperature benchmark is Morrow County (L6 S5). It has $R_{2-10} = 0.399$ and an estimated effective temperature of deformation of $\sim 700^\circ\text{C}$ [1], based on the presence of TEM-observed microstructures that experimentally occur at ~ 700 - 800°C , which is consistent with the temperature increase (~ 700 - 900°C) calculated from Hugoniot data for shock stage S5 chondrites [6]. An error of $\pm 100^\circ\text{C}$ is assigned to acknowledge variations in the temperatures given above. The high-temperature benchmark is the coarse (phenocryst) fraction of NWA 11993. It has $R_{2-10} = 0.880$, and an estimated deformation temperature of $\sim 1225^\circ\text{C}$, based on mantle equilibration temperatures of ~ 1160 - 1300°C for various ureilites [7,8], and based on the inference that most ureilites were shocked at magmatic temperatures during catastrophic disruption and global unroofing of the ureilite parent body [7,9]. An error of $\pm 75^\circ\text{C}$ is assigned to accommodate all the possible likely temperatures.

Results: Using the benchmarks for R_{2-10} and temperature and assuming a linear relationship between these values, we find $T_{\text{deform}} (^\circ\text{C}) = 1091.5 \times (R_{2-10} - 0.399) + 700$, and $T_{\text{err}} (^\circ\text{C}) = 0.0476 \times (1225 - T_{\text{deform}}) + 75$, where T_{deform} = effective deformation temperature and $T_{\text{err}} = \pm 1\sigma$ error. The model should be applicable to olivine in shock-deformed rocks with approximately $600^\circ\text{C} \leq T_{\text{deform}} \leq 1250^\circ\text{C}$. Fig. 2 shows data in a ternary plot of $f_{\langle 210 \rangle}$ ($\langle 210 \rangle$ is roughly halfway between $\langle 100 \rangle$ and $\langle 010 \rangle$ in the CRA diagram), $f_{\langle 100 \rangle}$, and $f_{\langle 010 \rangle} + f_{\langle 001 \rangle}$. We use this ternary because it illustrates that variations occur primarily in $[f_{\langle 010 \rangle} + f_{\langle 001 \rangle}] / f_{\langle 100 \rangle}$ ratio, which is related to R_{2-10} , and not to $f_{\langle 210 \rangle}$ values. This allows isotherms to be drawn radial to the $\langle 210 \rangle$ apex. Type 6 chondrites that were previously inferred [1] to have been shocked at elevated tempera-

tures of ~800-1000 °C (Miller (MIL) Range 99301, Kernouvé, Portales Valley) have $T_{\text{deform}} \sim 880-970$ °C, and those that were previously inferred [1] to have been shocked at low temperatures of ~650°C (Bruderheim) and ≤ 600 °C (Leedey) give appropriate temperatures within error, which suggest the model is valid. Other type 6 chondrites, Saint Severin and Park, were deformed hotter (~1130-1140 °C). Notable in Fig. 2 are lower R_{2-10} values for ureilites NWA 12433 and NWA 7630, which imply subsolidus deformation, and lower R_{2-10} values for the fine-grained fractions compared to the coarser-grained fractions in ureilites NWA 11993 and NWA 7630, which imply intrameteorite variability in deformation conditions. Although impacts occurring after catastrophic disruption might have occurred, we speculate that elevated fluid content, such as with the C-H-O-S fluid advocated for ureilites to drive reduction [10], could have acted similar to water-rich fluids [4, 5] to enhance *c*-type slip to result in lower R_{2-10} values for some ureilites, especially in fluid-enriched interstitial regions.

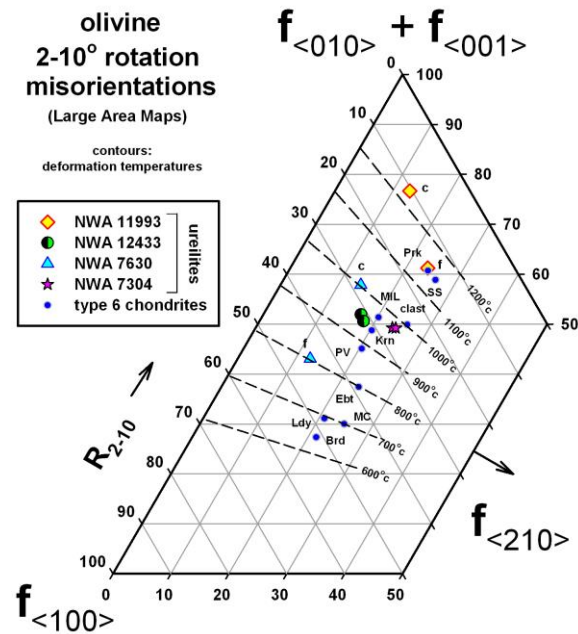


Fig.2. Rotation misorientation data for olivine in type 6 ordinary chondrites [1,2] and ureilites. Abbreviations: Brd = Bruderheim, Ldy = Leedey, MC = Morrow County, Ebt = Elbert, PV = Portales Valley, Krn = Kernouvé, MIL = MIL 99301, clast = melt clast in MIL 99301, SS = Saint Severin, Prk = Park, c = coarse fraction and f = fine-fraction in ureilites.

Excluding the data for ureilites with uncertain interpretation, Fig. 3 shows weighted shock stages [11] and model deformation temperatures separately for

shock-reheated and shocked-while-warm meteorites. For shock-reheated meteorites and the melt clast in MIL 99301 [1,2], Fig. 3a implies stronger shocks (S3.8-S6) can result in brief reheating temperatures of ~600-1000 °C, with higher temperatures for stronger shocks. For the shocked-while-warm meteorites [1,2], Fig. 3b implies no such correlation, with a mixture of lower (S1.1-S3.5) shock stages occurring in meteorites that were at ambient temperatures of ~900-1200 °C.

Acknowledgement: Grant support from NASA (grant 80NSSC19K0517) and from Portland State University (index FWAAXR) is gratefully acknowledged.

References: [1] Ruzicka A.M. & Hugo R.C. (2018) *GCA* **234**, 115-147. [2] Hugo R.C. et al. (2020) *MaPS* **55**, 1418-1438. [3] Carter N.L. and Ave'Llallemant H.G. (1970) *GSA Bull* **81**, 2181-2202. [4] Karato S.-i. et al. (2008) *Ann. Rev. Earth Planet. Sci.* **36**, 59-95. [5] Chatzaras V. et al. (2016) *JGR Solid Earth* **121**, 4859-4922. [6] Stöffler, D. et al. (1991) *GCA* **55**, 3845-3867. [7] Herrin J.S. et al. (2010) *MaPS* **45**, 1789–1803. [8] Singletary S.J. & Grove T.L. (2003) *MaPS* **38**, 95-108. [9] Rai N. et al. (2020) *Geochem. Persp. Lett.* **14**, 20-25. [10] Langendam A. et al. (2021) *MaPS* **56**, 2062-2082. [11] Jamsja N. & Ruzicka A. (2010) *MaPS* **45**, 828-849.

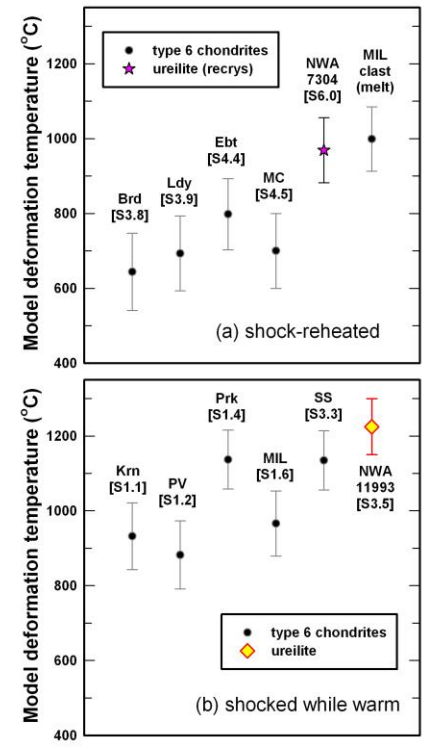


Fig. 3. Model deformation temperatures. Abbreviations as in Fig. 2. Brackets show weighted shock stage.